Science
AAAS

Experimental Observations of Stress-Driven Grain Boundary Migration

T. J. Rupert, *et al.*

Science **326**, 1686 (2009);
DOI: 10.1126/science.1178226

Science (print ISSN 0036-8075; online ISSN 1095-9203) is published weekly, except the last week in December, by the American Association for the Advancement of Science, 1200 New York Avenue NW, Washington, DC 20005.

21. E. A. Burt *et al.*, *Phys. Rev. Lett.* **79**, 337 (1997).
22. E. Nielsen, J. H. Macek, *Phys. Rev. Lett.* **83**, 1566 (1999).
23. B. D. Esry, C. H. Greene, J. P. Burke, *Phys. Rev. Lett.* **83**, 1751 (1999).
24. J. Schuster *et al.*, *Phys. Rev. Lett.* **87**, 170404 (2001).
25. J. P. D'Incao, H. Suno, B. D. Esry, *Phys. Rev. Lett.* **93**, 123201 (2004).
26. J. P. D'Incao, C. H. Greene, B. D. Esry, *J. Phys. B* **42**, 044016 (2009).
27. N. P. Mehta, S. T. Rittenhouse, J. P. D'Incao, J. von Stecher, C. H. Greene, *Phys. Rev. Lett.* **103**, 153201 (2009).
28. J. P. D'Incao, J. von Stecher, C. H. Greene, *Phys. Rev. Lett.* **103**, 033004 (2009).
29. T. Köhler, K. Góral, P. S. Julienne, *Rev. Mod. Phys.* **78**, 1311 (2006).
30. P. Massignan, H. T. C. Stoof, *Phys. Rev. A* **78**, 030701 (2008).
31. In ramping from $-200a_0$ to $a < -3000a_0$, we observe an increase in the axial size of the thermal cloud that is consistent with a temperature increase of the cloud to ~3 μK. During the trap-loss measurements, we observe negligible change in the Gaussian width of the thermal cloud (*17*).
32. We thank E. Olson for his contributions to this project and acknowledge useful discussions with E. Braaten, J. P. D'Incao, C. H. Greene, N. P. Mehta, and H. T. C. Stoof. Support for this work was provided by the NSF, Office of Naval Research, the Keck Foundation, and the Welch Foundation (grant C-1133).

Supporting Online Material
www.sciencemag.org/cgi/content/full/1182840/DC1
Materials and Methods
Figs. S1 to S4
References

5 October 2009; accepted 5 November 2009
Published online 19 November 2009;
10.1126/science.1182840
Include this information when citing this paper.

Experimental Observations of Stress-Driven Grain Boundary Migration

T. J. Rupert,[1,2] D. S. Gianola,[1,3] Y. Gan,[4] K. J. Hemker[1]*

In crystalline materials, plastic deformation occurs by the motion of dislocations, and the regions between individual crystallites, called grain boundaries, act as obstacles to dislocation motion. Grain boundaries are widely envisaged to be mechanically static structures, but this report outlines an experimental investigation of stress-driven grain boundary migration manifested as grain growth in nanocrystalline aluminum thin films. Specimens fabricated with specially designed stress and strain concentrators are used to uncover the relative importance of these parameters on grain growth. In contrast to traditional descriptions of grain boundaries as stationary obstacles to dislocation-based plasticity, the results of this study indicate that shear stresses drive grain boundaries to move in a manner consistent with recent molecular dynamics simulations and theoretical predictions of coupled grain boundary migration.

The strength and ductility of materials are inherently related to processes that govern the way that atoms move past one another, and, in crystalline metals, plastic deformation is most often associated with the way that dislocations (linear crystalline defects) move through individual crystals called grains. The mechanical behavior of metals and alloys can be tailored by introducing microstructural obstacles to dislocation motion; solid solution strengthening, precipitation hardening, and grain boundary strengthening are all examples of this. The latter is related to the fact that dislocation glide in polycrystalline metals is limited by the presence of grain boundaries and the misorientation between grains that they embody. The general realization that smaller grain-sized materials (possessing a higher density of grain boundaries) are stronger has lead to the often-cited Hall-Petch relation, which states that strength scales with the reciprocal square root of grain size (*1*, *2*) and assumes that grain boundaries act as obstacles to plastic deformation within the material.

[1]Department of Mechanical Engineering, Johns Hopkins University, Baltimore, MD 21218, USA. [2]Department of Materials Science and Engineering, Massachusetts Institute of Technology, Cambridge, MA 02139, USA. [3]Department of Materials Science and Engineering, University of Pennsylvania, Philadelphia, PA 19104, USA. [4]Institute for Materials Research II, Karlsruhe Institute of Technology, 76131 Karlsruhe, Germany.

*To whom correspondence should be addressed. E-mail: hemker@jhu.edu

Materials scientists traditionally describe the detailed geometric structure of grain boundaries through a coincident site lattice (CSL), which promotes the view of grain boundaries as mechanically static, immovable structures. However, recent studies involving nanocrystalline materials have introduced convincing evidence to suggest that grain boundaries are not static; mechanically induced room temperature grain growth has been associated with indentation (*3*–*5*), compression (*6*, *7*), and tensile loading (*8*–*11*). These observations cannot be described by classical models of grain growth (*8*) and were originally characterized as strain-driven grain boundary migration (*4*). Subsequent experiments quantifying grain growth in terms of temperature (*5*), strain rate (*10*), proximity to crack tips (*12*), and testing mode (*7*) suggested that grain boundary migration in nanocrystalline metals may be driven more by stress than by plastic strain. The experiments outlined below demonstrate that the room-temperature grain growth observed in nanocrystalline metals is associated with shear stress-driven grain boundary migration, thereby confirming recent theories of coupled grain boundary migration (*13*, *14*) and confirming that grain boundaries are not static structures as traditionally assumed.

It is widely acknowledged that shear stresses drive dislocation motion. The motion of low-angle grain boundaries, which consist of dislocation arrays, under shear stress can be described by the collective movement of the individual dislocations in these boundaries (*15*, *16*). By contrast, the concept of shear stress moving a high-angle grain boundary is relatively foreign to the materials science community, with experimental observations of such a mechanism being elusive. Cahn and co-workers (*13*) have recently published a unified theory of coupled grain boundary motion based on the supposition that the normal motion of a grain boundary couples to the tangential displacement (shear) of adjacent grains. Molecular dynamics simulations (*14*, *17*) and bicrystal experiments (*18*–*20*) involving the migration of specific high-angle tilt boundaries have been shown to be consistent with Cahn's theory of coupled boundary migration. Recent molecular dynamics simulations (*21*) suggest that a fraction of general grain boundaries do exhibit anomalously high mobility when operating in a shear coupled mode, but experimental extensions to a more general population of boundaries, where grain boundaries are composed of a combination of twist and tilt character and bounded by grain boundary junctions, have proven much harder to realize. Moreover, the need for measurable grain boundary mobility requires that the bicrystal experiments be done at elevated temperature, making the separation of mechanical and thermal effects problematic. The occurrence of room-temperature grain growth in nanocrystalline metals offers the opportunity to impose much higher stresses on a much wider range of boundaries without the superposition of elevated temperature. This study was specifically designed to test the hypothesis that shear stresses can directly cause high-angle grain boundaries to move. The experiments described here allowed the investigation of the influence of normal and shear stresses and strains on the motion of a wide population of grain boundaries as encountered in most polycrystalline materials, without the need to characterize adjacent nanocrystalline grains and boundaries with high fidelity.

In order to elucidate the effect of stress and strain on mechanically induced grain growth, we have borrowed a page from the fracture mechanics community, where geometric concentrators have been used to discriminate between stress-controlled brittle fracture and strain-controlled ductile fracture (*22*, *23*). We present experiments on freestanding nanocrystalline Al thin films, where spatial variations in the stress and strain states were deliberately introduced by using special sample geometries. A major benefit of our approach lies in

the ability to study a statistical ensemble of grains and their evolution because the individual grains are much smaller than the gradients of the stress and strain fields. This allowed us to collect sufficient data from transmission electron microscopy (TEM) to statistically characterize how microstructure evolves under a specific deformation field. Combining systematic and quantitative microstructural analysis with continuum descriptions of stress and strain gradients allowed us to distinguish between the effects of stress and strain on grain growth.

Microtensile free-standing thin film specimens with hole patterns (50-μm radius) in the gage section (700 μm by 4 mm) were fabricated as shown in Fig. 1, A and B, deformed, and examined by using post-mortem TEM. All films were deposited to thicknesses of 150 to 220 nm by using pulsed electron beam evaporation, which limited the growth of through-thickness grains and yielded average grain sizes of 60 to 90 nm with large numbers of high-angle boundaries and no preferred crystallographic texture (Fig. 1, C and D). Observations of room-temperature grain growth in undeformed nanocrystalline materials have been reported [see, for example, (*24*)], but the films used in the current study were stable at room temperature and showed no evidence of spontaneous thermal grain growth. Interior holes were added to traditional tensile geometries with photolithography and used to exploit the fact that, with local yielding, the maximum strain occurs at the hole edge while the maximum stress is offset from the edge (*22*, *23*, *25*). In this way, a specimen with two holes situated horizontally (referred to as the horizontal-hole geometry) (Fig. 1A) was used to study and contrast the effects of stress and strain on grain growth. The influence of stress state was studied by patterning two holes collinearly at a 45° angle from the tensile axis (referred to as the angled-hole geometry) (Fig. 1B); the overlapping stress fields resulted in well-separated regions of increased shear and normal stresses. For both types of specimens, the gradients in stress and strain exist on a much larger scale (tens of micrometers) than the length scale associated with the material microstructure (tens of nanometers), meaning a large number of grains felt the altered stress or strain state. Although plastic strain can introduce local heterogeneities on the order of the microstructure, statistical averaging of grain growth over areas that contain hundreds of grains is expected to mitigate the influence of these local perturbations. Spatial variations in grain growth were quantified by using bright field TEM images to obtain grain size distributions at different specimen positions. Over 100 grain sizes were measured for each data set, and Welch's *t* test was used to ensure that the observed measurements of grain growth were statistically significant. Trends in grain growth for multiple specimens and specimen geometries were then reconciled with the results of finite element analysis (FEA), which predicted the full-field stress and strain distributions in the various specimens and included the effects of stress-induced wrinkling in freestanding thin films (figs. S1 and S2). Details for the experimental tensile setup and FEA can be found in (*26*).

Horizontal-hole specimens were first used to measure the relative importance of stress and strain in driving mechanically induced grain growth. Remote axial displacements of 25 to 30 μm were applied to the specimens, and the corresponding stress and strain fields were calculated by using a finite element mesh of the specimen, plasticity laws determined from uniaxial tensile experiments, and contributions from mechanical wrinkling (displacements out of the plane of the specimen). The stress and strain contours predicted by the FEA are shown in Fig. 2. The maximum normal and shear stresses both rise gradually with increasing distance from the hole perimeter, reach a local maximum at about half of the hole radius (~25 μm), and fall off beyond this point. It should be noted that the heterogeneity and asymmetry in the stress and strain fields arise because of wrinkling-induced relaxations and local plasticity. By contrast, the maximum normal and distortional plastic strains were found to be highest at the edge of the hole and to fall off rapidly away from that edge. The grain growth was characterized in two well-defined regions: region 1, where the strains are greatest, and region 2, where the stresses are highest. The measured grain size distributions are summarized in Fig. 2, where cumulative distribution plots (Fig. 2F) illustrate the fact that grain growth occurred in both regions but was greatest in region 2. This finding points to the role of stress in promoting grain growth. Additional statistical parameters for characterizing the microstructure of each region, along with average stress and strain values from FEA, can be found in table S1.

Having clarified that the observed mechanical grain growth is driven by stress, we next investigated the relative importance of shear stresses in promoting this growth. Angled-hole specimens were studied to separate the regions where deformation is dominated by normal stresses from those where shear dominates. Our TEM observations were made after the specimen had undergone a complex deformation path; selecting stresses as the variables of interest would ignore previous deformation history and nonmonotonic behavior, both of which are important when the specimen wrinkles. Accordingly, it is important to consider the overall contribution of the stresses over the duration of the test, which is captured by energy quantities that include the history of the stresses. Therefore, we analyzed the simulations of this geometry in terms of the cumulative contributions of volumetric and distortional energy density incurred by the specimen, with these quantities being directly related to the normal and shear stresses, respectively (*26*). As demonstrated by the FEA shown in Fig. 3, applying a remote displacement of 25 μm to the angled-hole specimen resulted in a substantial enhancement of the distortional energy density in the region between the holes, whereas the volumetric energy density in this region was not strongly magnified by the presence of neighboring holes. Of the three regions quantitatively investigated for these specimens (Fig. 3B), region 2 had the highest distortional energy density, whereas region 1 incurred a higher distortional energy

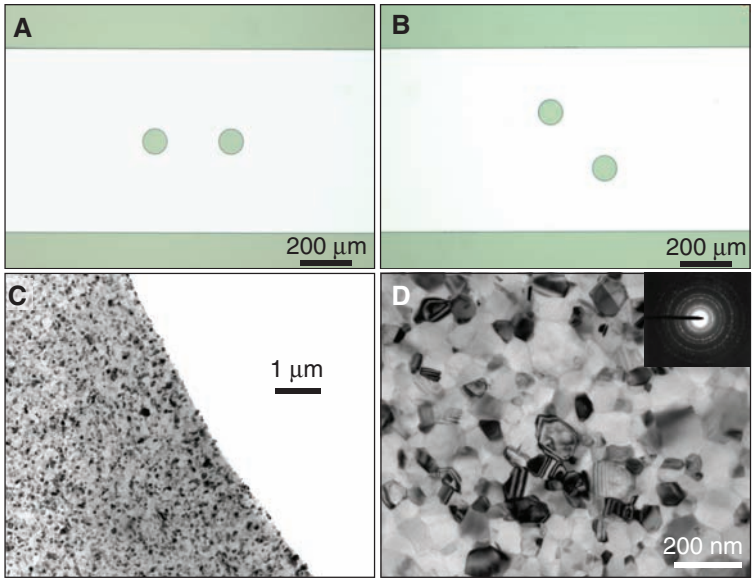

Fig. 1. Microfabrication techniques and electron beam evaporation were used to make thin-film tensile specimens with thicknesses ranging from 150 to 220 nm and mean grain sizes of 60 to 90 nm. The introduction of holes at horizontal (**A**) and angled orientations (**B**) produces complex stress and strain fields within the film when it is pulled in tension. Closer inspection of one of these holes in the TEM (**C**) shows submicrometer resolution at the hole edge and a microstructure that exists on a length scale orders of magnitude smaller than that associated with the sample geometry. Bright field TEM imaging at a higher magnification (**D**) shows a random microstructure with overlapping grains and high-angle grain boundaries.

density than region 3. Volumetric energy densities in regions 2 and 3 were about the same but lower than in region 1 (Fig. 3C), whereas all three were substantially lower than the distortional values. Post-mortem TEM measurements of these regions are summarized in Fig. 3D, where grain size distributions for each region and the as-deposited material are presented as cumulative distribution plots (additional characterization parameters are available in table S1). Inspection of these distributions shows systematic differences in grain growth. The highest average grain size and, correspondingly,

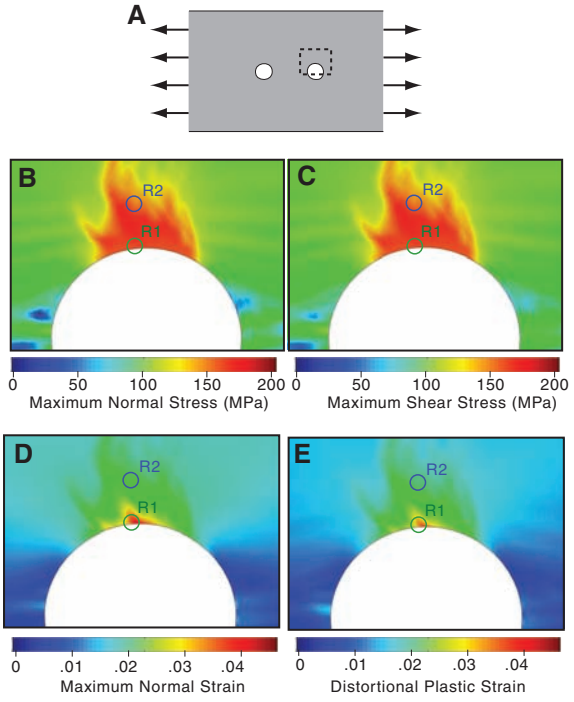

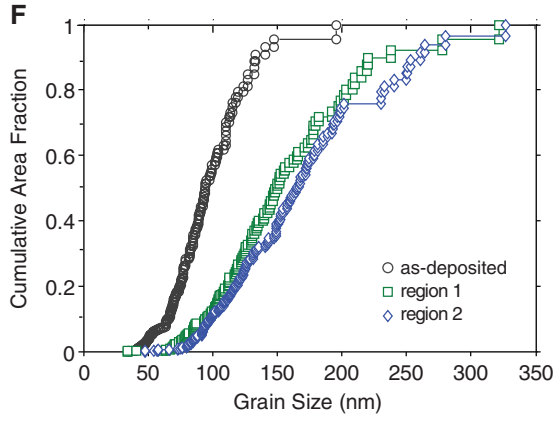

Fig. 2. Finite element simulations were used to investigate stress and strain fields in a region near the hole of a 170nm-thick horizontal-hole specimen (**A**). Contour plots of the maximum normal stress (**B**), maximum shear stress (**C**), maximum normal strain (**D**), and distortional plastic strain (**E**) are presented here. Regions of interest that were investigated in the TEM are denoted in the contour plots. The microstructure in each region was measured and compared with the as-deposited grain size distribution in the form of area-weighted cumulative distribution plots (**F**). Grain growth is highest away from the hole edge, showing that stress drives this microstructural evolution.

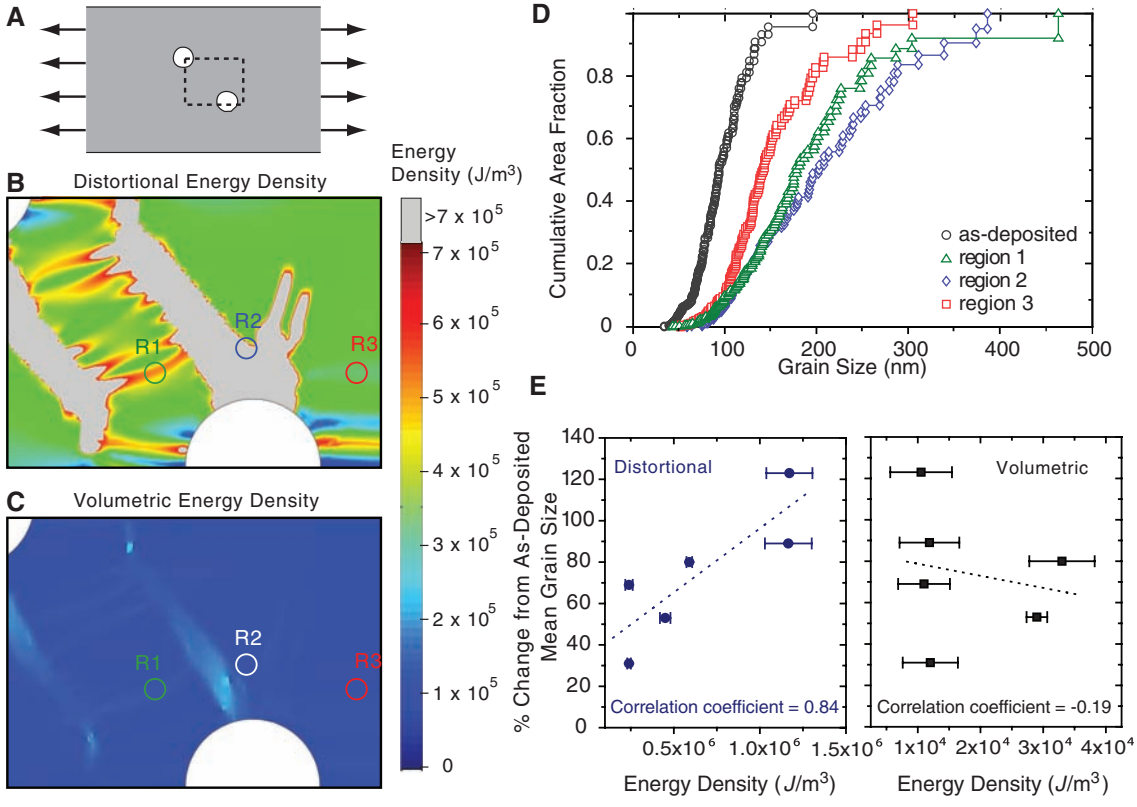

Fig. 3. The angled-hole geometry was modeled with finite element simulations to investigate the normal and shear stresses in the areas around and between the holes (**A**). The distributions of the distortional energy density (dominated by shear stresses) (**B**) and the volumetric energy density (dominated by normal stresses) (**C**) are presented by using contour plots. The gray areas represent areas where the energy density is higher than ~7×10^5 J/m^3. Regions of interest which were investigated in the TEM are denoted in the contour plots, with the microstructure in these regions presented as cumulative distribution plots of the area-weighted grain size (**D**). Correlations between energy density quantities and grain growth are examined (**E**), revealing a positive correlation between the extent of grain growth and distortional energy density, whereas no such relationship exists between grain growth and volumetric energy density. The error bars in (E) represent the standard deviation of the energy quantities from FEA over the regions where grain size statistics (~1000 grain sizes measured for these plots) were collected, whereas the dotted lines represent linear fits to the data to show general trends. These plots show that grain growth scales more closely with the trends in distortional energy density, pointing to shear stress as the driving force for the grain boundary migration during grain growth.

the most severe grain growth were measured in region 2, where only the distortional energy density term is the greatest. Direct comparison of regions 1 and 3 indicates that region 1 experienced markedly more grain growth than region 3. Taken as a whole, the measurements collected on multiple angled-hole specimens indicate that grain growth scaled with shear stresses that produce distortional work, with the grain size distribution displaying the most grain growth belonging to region 2, followed by region 1, and then region 3. By contrast, the hypothesis that normal stresses control grain growth would have predicted that growth in regions 2 and 3 would have been nearly the same and smaller than the growth in region 1, which is contrary to our observations. Figure 3E summarizes the results from two independent angled-hole specimens, with grain growth plotted versus the energy density terms. The dotted lines represent linear fits to the data, with the accompanying correlation coefficient for each fit provided at the bottom of the graph. From Fig. 3E, a positive correlation emerges between grain growth and distortional energy density, whereas grain growth does not appear to scale with increasing volumetric energy density. These results point to shear stress as the driving force for mechanically induced grain boundary migration.

Further insight into the mechanism of mechanical grain growth can be gained by analyzing changes in grain shape and the evolution of grain size distributions for the specimens discussed above as well as similar samples from slightly different deposition batches (*26*). Figure 4A shows that the aspect ratios of measured grains do not scale with the amount of growth experienced by the material. The fact that the grains remain essentially equiaxed (within the range of 1.3 to 1.5) precludes diffusion-controlled processes such as Coble creep (*27*). The grain growth observed in this study is also characterized by a grain size distribution that broadens as grain size increases (Fig. 4B), as opposed to a pure shift in the distribution toward larger grain sizes as would be expected for normal thermally driven grain growth (*28*) or the grain growth observed in superplastic deformation (*29*, *30*). Evidence for inhomogeneous growth, where certain grains grow preferentially at the expense of others, can also be found in the combined cumulative distribution plots (Figs. 2F and 3D). The finding that all of the grain size distributions start at the same minimum size indicates that small grains still exist within the evolved microstructure, although they represent a decreasing fraction of the material as grain growth progresses.

Although traditional grain growth mechanisms fail to explain the grain growth characterized in this study, the finding that grain growth scales with applied stress is in agreement with recent theoretical descriptions and molecular dynamics simulations (*13*, *14*) of coupled grain boundary migration. Snapshots of local tilt boundary behavior during the molecular dynamics simulations suggest that distortions of structural units consisting of only a few atoms produce the shear and attendant normal boundary motion. These simulations further illustrate that the coupling factor, β, which relates normal and tangential motion of a grain boundary, is geometrically related to the misorientation angle, even for high-angle boundaries (*14*). The original simulations focused on high-symmetry tilt boundaries (*13*, *14*), but more recent simulations suggest that the shear coupling occurs in more general boundaries as well (*31*, *32*, *21*). To date, experimental evidence of the coupling has been restricted to low- and high-angle tilt boundaries (*18*–*20*). The exact orientation of individual grains and grain boundaries could not be determined in the current study because there are multiple grains through the thickness of the film, but one advantage of the use of nanocrystalline samples lies in the fact that grain growth and, by inference, grain boundary migration were observed for a wide range of grain boundary characters. The finding that coupled boundary migration is not limited to tilt boundaries is especially intriguing.

This experimental confirmation of stress-driven migration of general grain boundaries is supported by recently published in situ TEM observations of ultrafast grain boundary motion in nanocrystalline (*12*) and ultrafine-grained Al (*33*). The in situ observations show the rapid motion of curved and nonspecific grain boundaries, but only under the influence of an applied stress. In situ measurements of the shear strain associated with grain boundary migration confirm the existence of a coupling factor in the case of a low-index grain boundary, but the measured values of this coupling were smaller than those predicted by Cahn. A more generalized geometric model of shear coupling, which is consistent with Cahn's model and with a grain boundary dislocation-based representation of grain boundary migration (*34*), has been derived to explain the in situ observations (*35*). The specific details of these coupled boundary migration models are still under debate, but the general conclusion of the current work, that shear stresses promote coupled grain boundary migration and grain growth in nanocrystalline Al, is fully consistent with all three geometric models.

The experimental finding that a general population of grain boundaries can be mobile during deformation contrasts with the generally accepted notion that grain boundaries act as stationary obstacles within a microstructure. Material scientists traditionally view the mechanics of grain boundaries in terms of the Hall-Petch relation (*1*, *2*), which states that a material's strength increases with decreasing grain size. The most common explanation of this trend describes grain boundaries as obstacles to the transfer of dislocations (and, therefore, plastic strain) between adjacent crystals. Although this is true for coarse-grained and microcrystalline materials, the grain boundary migration observed here demonstrates that grain boundaries in nanocrystalline materials can be responsible for a very different response, in fact accommodating plastic strain. The grain boundary motion itself represents a permanent transfer of material, with the lattice undergoing irreversible shear within the volume traversed by

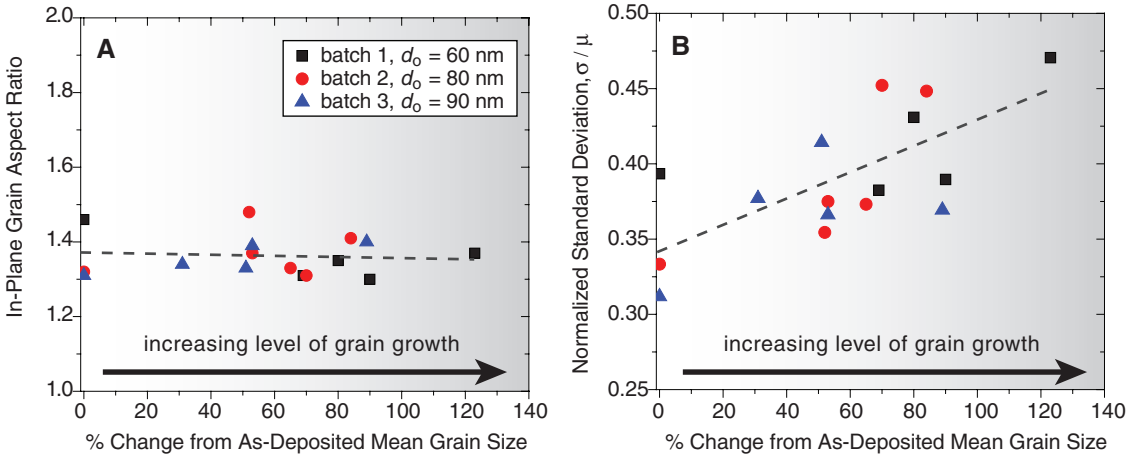

Fig. 4. Compilation plots quantifying the microstructural evolution observed in various specimens and specimen geometries (each data point represents over 100 grain size measurements). The labels batch 1, 2, and 3 represent different deposition batches with slightly different as-deposited average grain sizes (d_o = 60, 80, and 90 nm, respectively), whereas the dotted lines represent linear fits to the data points to show general trends. The aspect ratios of the grains do not change as a result of of grain growth (**A**). The normalized standard deviation increases with the level of grain growth (**B**), which is a signature of a grain size distribution that broadens as grain size increases. These results contrast with signatures of grain growth caused by thermal driving forces, diffusional creep, or superplastic deformation.

the boundary without the need for dislocation slip events. In addition to acting as a direct mechanism for plastic flow, coupled grain boundary migration creates larger grains within the microstructure, which allows microscale plasticity mechanisms (normal dislocation plasticity) to become active (*8*).

Having pinpointed shear stress as the driving force governing mechanically induced grain growth, it is worth asking what role stress-driven grain boundary migration plays in governing materials behavior. The microstructural instability noted in nanocrystalline materials (*3*–*12*) indicates that grain boundary migration can result in mechanical behavior that is not only different from microcrystalline materials but dynamic as well. This departure from conventional plasticity is no doubt associated with the high stresses that nanocrystalline metals can accommodate. In conventional polycrystalline materials, the onset of dislocation-based plasticity limits the stresses that can be applied; nevertheless, it is reasonable to conclude that there may be hereto overlooked situations where stress-driven boundary migration influences the mechanical response and microstructural stability of other materials as well.

References and Notes

1. E. O. Hall, *Proc. Phys. Soc. B* **64**, 747 (1951).
2. N. J. Petch, *J. Iron Steel Inst. London* **174**, 25 (1953).
3. M. Jin, A. M. Minor, E. A. Stach, J. W. Morris Jr., *Acta Mater.* **52**, 5381 (2004).
4. M. Jin, A. M. Minor, J. W. Morris Jr., *Thin Solid Films* **515**, 3202 (2007).
5. K. Zhang, J. R. Weertman, J. A. Eastman, *Appl. Phys. Lett.* **87**, 061921 (2005).
6. D. Pan, S. Kuwano, T. Fujita, M. W. Chen, *Nano Lett.* **7**, 2108 (2007).
7. S. Brandstetter, K. Zhang, A. Escuadro, J. Weertman, H. Van Swygenhoven, *Scr. Mater.* **58**, 61 (2008).
8. D. S. Gianola *et al.*, *Acta Mater.* **54**, 2253 (2006).
9. G. J. Fan, L. F. Fu, H. Choo, P. K. Liaw, N. D. Browning, *Acta Mater.* **54**, 4781 (2006).
10. D. S. Gianola, D. H. Warner, J. F. Molinari, K. J. Hemker, *Scr. Mater.* **55**, 649 (2006).
11. D. S. Gianola, C. Eberl, X. M. Cheng, K. J. Hemker, *Adv. Mater.* **20**, 303 (2008).
12. M. Legros, D. S. Gianola, K. J. Hemker, *Acta Mater.* **56**, 3380 (2008).
13. J. W. Cahn, J. E. Taylor, *Acta Mater.* **52**, 4887 (2004).
14. J. W. Cahn, Y. Mishin, A. Suzuki, *Acta Mater.* **54**, 4953 (2006).
15. C. H. Li, E. H. Edwards, J. Washburn, E. R. Parker, *Acta Metall.* **1**, 223 (1953).
16. D. W. Bainbridge, C. H. Li, E. H. Edwards, *Acta Metall.* **2**, 322 (1954).
17. V. A. Ivanov, Y. Mishin, *Phys. Rev. B* **78**, 064106 (2008).
18. M. Winning, G. Gottstein, L. S. Shvindlerman, *Acta Mater.* **49**, 211 (2001).
19. M. Winning, G. Gottstein, L. S. Shvindlerman, *Acta Mater.* **50**, 353 (2002).
20. D. A. Molodov, V. A. Ivanov, G. Gottstein, *Acta Mater.* **55**, 1843 (2007).
21. D. L. Olmsted, E. A. Holm, S. M. Foiles, *Acta Mater.* **57**, 3694 (2009).
22. R. Ritchie, J. Knott, J. Rice, *J. Mech. Phys. Solids* **21**, 395 (1973).
23. R. K. Nalla, J. H. Kinney, R. O. Ritchie, *Nat. Mater.* **2**, 164 (2003).
24. V. Y. Gertsman, R. Birringer, *Scr. Metall. Mater.* **30**, 577 (1994).
25. J. Griffiths, D. Owen, *J. Mech. Phys. Solids* **19**, 419 (1971).
26. Materials and methods are available as supporting material on *Science* Online.
27. R. L. Coble, *J. Appl. Phys.* **34**, 1679 (1963).
28. G. Gottstein, L. S. Shvindlerman, *Grain Boundary Migration in Metals: Thermodynamics, Kinetics, Applications* (CRC, Boca Raton, FL, 1999).
29. M. F. Ashby, R. A. Verrall, *Acta Metall.* **21**, 149 (1973).
30. O. Sherby, J. Wadsworth, *Prog. Mater. Sci.* **33**, 169 (1989).
31. N. Bernstein, *Acta Mater.* **56**, 1106 (2008).
32. H. Zhang, D. Du, D. J. Srolovitz, *Philos. Mag.* **88**, 243 (2008).
33. F. Mompiou, D. Caillard, M. Legros, *Acta Mater.* **57**, 2198 (2009).
34. C. M. F. Rae, D. A. Smith, *Philos. Mag. A* **41**, 477 (1980).
35. D. Caillard, F. Mompiou, M. Legros, *Acta Mater.* **57**, 2390 (2009).

36. This work was supported by the U.S. Department of Energy, Office of Basic Energy Science and the NSF Nanoscale Interdisciplinary Research Team program (grant no. DMR-0210215). The authors are grateful for illuminating discussions with J. D. Embury and C. Eberl regarding the development of complex stress states in patterned thin films. D.S.G. acknowledges support from an Alexander von Humboldt postdoctoral fellowship.

Supporting Online Material

www.sciencemag.org/cgi/content/full/326/5960/1686/DC1
Materials and Methods
Figs. S1 and S2
Tables S1 and S2
References

25 June 2009; accepted 27 October 2009
10.1126/science.1178226

Real-Time Observation of Carbonic Acid Formation in Aqueous Solution

Katrin Adamczyk,[1] Mirabelle Prémont-Schwarz,[1] Dina Pines,[2] Ehud Pines,[2]* Erik T. J. Nibbering[1]*

Despite the widespread importance of aqueous bicarbonate chemistry, its conjugate acid, carbonic acid, has remained uncharacterized in solution. Here we report the generation of deuterated carbonic acid in deuterium oxide solution by ultrafast protonation of bicarbonate and its persistence for nanoseconds. We follow the reaction dynamics upon photoexcitation of a photoacid by monitoring infrared-active marker modes with femtosecond time resolution. By fitting a kinetic model to the experimental data, we directly obtain the on-contact proton-transfer rate to bicarbonate, previously inaccessible with the use of indirect methods. A Marcus free-energy correlation supports an associated pK_a (K_a is the acid dissociation constant) of 3.45 ± 0.15, which is substantially lower than the value of 6.35 that is commonly assumed on the basis of the overall carbon dioxide–to–bicarbonate equilibrium. This result should spur further exploration of acid-base reactivity in carbon dioxide–rich aqueous environments such as those anticipated under sequestration schemes.

Recent isolation of carbonic acid (H_2CO_3) in the gas and solid phases has conclusively disproved long-held claims of the molecule's intrinsic kinetic instability (*1*–*3*). Theoretical calculations have shown that H_2CO_3 only becomes unstable when water is present; that is, adding a single water molecule to anhydrous H_2CO_3 accelerates its simulated decomposition by a factor of 10^9 (*4*–*9*). Aqueous H_2CO_3 is understood to dissociate by a proton-relay mechanism that uses several catalyzing water molecules. For this reason, direct observation of aqueous H_2CO_3 has proven to be elusive, a situation that is somewhat surprising given the vital physiological role that the H_2CO_3/HCO_3^- buffer system has long been known to play in regulating the pH of blood and other biological fluids (*10*). Furthermore, sequestration plans to mitigate anthropogenic carbon dioxide emissions involve injecting several hundreds of gigatons of CO_2 into the oceans (*11*). Precise and reliable dissociation constants for carbonic acid over a wide range of ionic strengths, temperatures, and pressures will need to be established to determine in situ chemical behavior in such contexts (*12*–*14*).

In pure water (pH = 7 before CO_2 dissolution), aqueous solvation of CO_2 is understood to be accompanied by hydration, resulting in carbonic acid (H_2CO_3) (Eq. 1), and subsequent acid-base chemistry leading to bicarbonate (HCO_3^-) and carbonate (CO_3^{2-}) (Eq. 2)

$$CO_2(g) + 3H_2O \rightleftarrows CO_2(aq) + 3H_2O \rightleftarrows H_2CO_3 + 2H_2O \quad (1)$$

$$H_2CO_3 + 2H_2O \rightleftarrows HCO_3^- + H_3O^+ + H_2O \rightleftarrows CO_3^{2-} + 2H_3O^+ \quad (2)$$

The net result is a decrease in pH. Conversely, bicarbonate acts as a moderately weak base in solutions below neutral pH; titrations on time scales extending to minutes afford an effective pK_a (K_a is the acid dissociation constant) value

[1]Max Born Institut für Nichtlineare Optik und Kurzzeitspektroskopie, Max Born Strasse 2A, D-12489 Berlin, Germany. [2]Department of Chemistry, Ben-Gurion University of the Negev, Post Office Box 653, Beer-Sheva 84105, Israel.

*To whom correspondence should be addressed. E-mail: epines@bgu.ac.il (E.P.); nibberin@mbi-berlin.de (E.T.J.N.)